Experimental Investigation of the Speed of a Shockwave

Trae Nelson[1] | Zakary Steenhoek[1] | Justin Ritzenthaler[1] | Colin McArthur[1] | Nicolas Nelson[1]

Arizona State University, Tempe, AZ, 85288, United States

The purpose of this experiment is to investigate the speed of a shock wave using a shock tube. A brief overview of the procedure of this experiment goes as follows. Ambient pressure and temperature are first recorded along with their corresponding uncertainties. After this, instruments are checked to make sure they are on and running. Necessary information such as position of the pressure transducers is recorded as well. After these steps, the tests begin. The following steps are repeated with a new material as the diaphragm for each run. For each run, the diaphragm is installed, and the bolts are tightened to seal the tube. After this, the air source and inlet valves are sealed, and the air hose is installed. Next, the source valve is opened, and the driver section of the shock tube is slowly pressurized until the diaphragm bursts. After the diaphragm bursts, the inlet valve is immediately closed. The air in the hose is then bled and the system is vented by opening the inlet valve. Finally, the bolts are removed, and the diaphragm is swapped out. The experimental results showed that a thicker diaphragm like 5mm plastic requires much more pressure to rupture and produces an asymmetrical shockwave due to the material rupturing non-uniformly. Aluminum ruptures under much less pressure and produces a more uniform shock wave. These results prove that stronger materials acting as the diaphragm produce larger pressure differentials between the two sections, resulting in shockwaves propagating faster through the tube. However, stronger materials tend to rupture non-uniformly causing asymmetrical shock waves, while weaker materials produce smaller pressure differentials and create a more uniform shock wave.

I. Nomenclature

a	=	Speed of sound (m/s)
a_{ana}	=	Analytical speed of sound (m/s)
a_{exp}	=	Experimental speed of sound (m/s)
a_1	=	Speed of sound in driven section 1 (m/s)
$a_{1,ana}$	=	Analytical speed of sound in driven section 1 (m/s)
$a_{4,ana}$	=	Analytical speed of sound in driving section 4 (m/s)
c_v	=	Specific heat (J/kg*K)
Δ	=	Change over time
δ	=	Uncertainty
e_1	=	initial specific internal energy (J/kg)
e_1	=	final specific internal energy (J/kg)
γ	=	Specific heat ratio
γ_a	=	Specific heat ratio for a given speed of sound
h_1	=	Initial specific enthalpy at state 1 (J/kg)
h_2	=	Final specific enthalpy at state 2 (J/kg)
M	=	Molecular mass (kg/mol)
m	=	Mass (kg)
M_s	=	Mach number of the shockwave

[1] Student, Arizona State University

p = Pressure (kPa)
p_1 = Pressure of state 1 in the driven section (kPa)
p_2 = Pressure of state 2 in the driven section (dynamic pressure transducer 2) (kPa)
p_4 = Pressure of state 4 or the driver section (kPa)
$p_{2,ana}$ = Analytical pressure of state 2 in the driven section (dynamic pressure transducer 2) (kPa)
$p_{2,exp}$ = Experimental pressure of state 2 in the driven section (dynamic pressure transducer 2) (kPa)
$\mathcal{R}$ = Universal gas constant (J/mol*K)
R = Specific gas constant (J/kg*K)
ρ = Density (kg/m^3)
ρ_1 = Initial density at state 1 (kg/m^3)
ρ_1 = Final density at state 2 (kg/m^3)
T = Temperature (K)
T_1 = Initial temperature at state 1 (K)
T_2 = Final temperature at state 2 (K)
T_a = Temperature for a given speed of sound a (K)
t = Time (ms)
u_p = Speed of contact surface (m/s)
$u_{p,ana}$ = Analytical speed of contact surface (m/s)
$u_{p,exp}$ = Experimental speed of contact surface (m/s)
u_1 = Speed of upstream gas (m/s)
u_2 = Speed of downstream gas (m/s)
v_1 = Initial specific volume at state 1 (m^3/kg)
v_2 = Final specific volume at state 2 (m^3/kg)
W = Speed of the shockwave (m/s)
W_{ana} = Analytical speed of the shockwave (m/s)
x = distance between dynamic pressure transducer (m)
y = arbitrary variable used as a placeholder for future variables

II. Introduction

A. Stationary Shockwave vs. Moving Shockwave

There are two key types of shockwaves that are of interest for this experiment. Those being stationary and moving shockwaves. Shockwaves are an irreversible phenomenon that can only form when there is flow moving faster than Mach 1. When the flow needs to suddenly decelerate, the laws of conservation of mass, momentum, and energy tell us that something sudden must happen in the flow to slow it down (i.e., a shockwave must be formed). Across a shockwave, the flow undergoes rapid increases in pressure, density, and temperature, while velocity decreases.
Stationary shockwaves are shockwaves that appear stationary in space relative to the laboratory. The shockwave in this case is propagating at a speed equal to the speed of the upstream flow. The stagnation temperature across a stationary shockwave remains constant. The properties of the flow field depend only on the position for a stationary shockwave. This flow is steady. Fig. 1 helps illustrate a stationary normal shockwave.

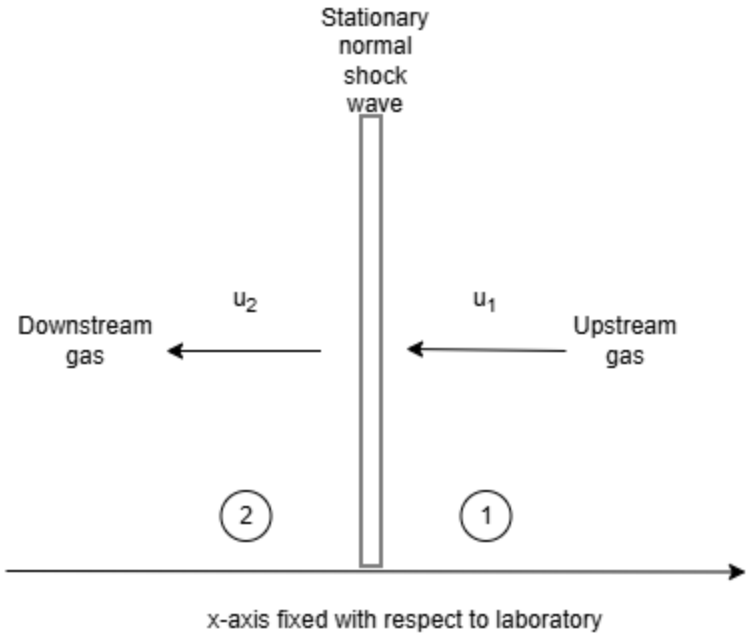

Fig. 1: Schematic showing a stationary normal shockwave.

Moving shockwaves differ from stationary shockwaves in the sense that the shockwave is now propagating through a medium and does not appear fixed relative to the laboratory. We let u_1 = 0 meaning the shockwave is no longer moving at the same speed as the upstream flow. The stagnation temperature across a moving shock can also increase due to the motion of the shock unlike a stationary shockwave. The properties of the flowfield depend on both time and position for a moving shockwave. This flow is unsteady wave motion. Fig. 2 helps illustrate a moving shockwave. The relative speed of the flow behind the moving shockwave (u_2) is equal to the difference between the speed of the moving shockwave (W) and the actual velocity of the flow behind the shockwave (u_p). [1]

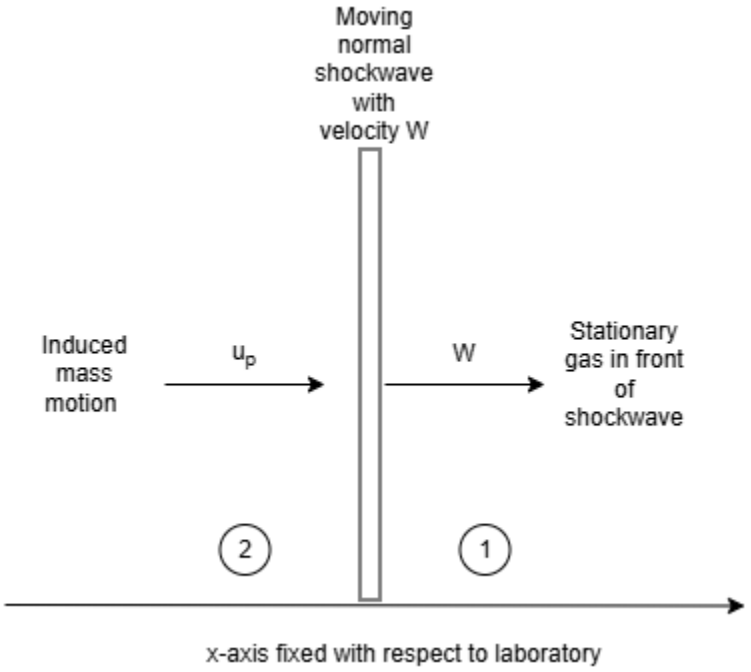

Fig. 2: Schematic showing a moving shockwave

B. Shock tube

Shock tubes allow us to apply and study unsteady wave motion. A shock tube is a tube that's sealed at both ends. A diaphragm separates a region of low-pressure gas on the right called the driven section (region 1) to a region of high-pressure gas on the left called the driver section (region 4). Fig. 3 shows the pressure distribution in the shock tube before the diaphragm ruptures. After the diaphragm ruptures, a shockwave propagates into region 1, while an expansion wave propagates into region 4. The motion of the shockwave to the right with a velocity of W causes the pressure of the gas behind it to increase. This induces mass motion with a velocity denoted as u_p. The contact surface is what we call the divide between the two gases after the diaphragm has ruptured. The contact surface moves at a velocity equal to u_p. Using different materials for the diaphragm allows for different configurations of gas pressure in each region. Diaphragm materials with higher strength will allow the driver section to build up more pressure than materials with less strength. [2]

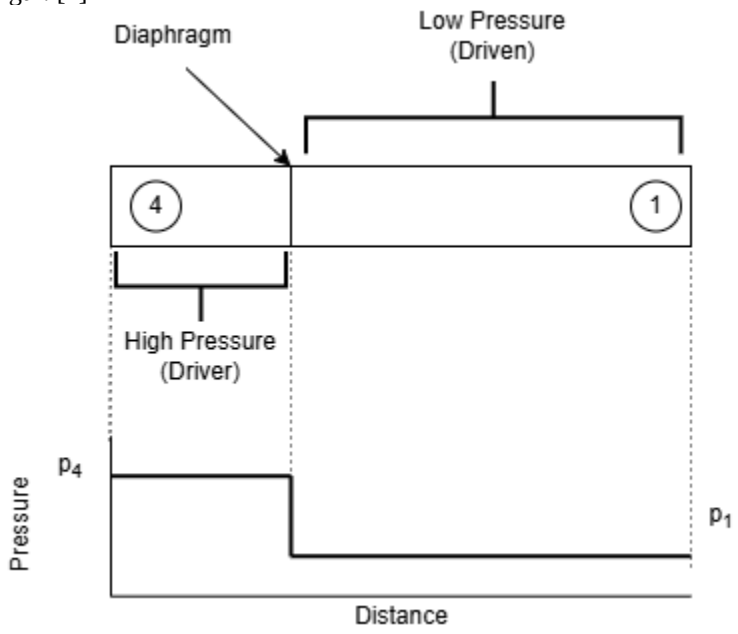

Fig. 3: Schematic of the shock tube before the diaphragm has burst with a plot of the pressure distribution shown underneath.

Fig. 4 in the procedure below illustrates what happens in the shock tube after the diaphragm ruptures.

III. Procedures

The following is a detailed description of the laboratory equipment used, and the procedures followed for experimental data collection and data processing used to carry out this experiment.

A. Experimental Equipment

The experimental equipment used includes a shock tube, various diaphragm materials, multiple pressure transducers, a digital thermocouple, and data collection software. Details about each piece of equipment can be found next:

I. ASU laboratory high-speed *shock tube*

The main piece of equipment used for this experiment is a shock tube, illustrated in Fig. [4]. This is a device used to induce shock waves and artificially create regions of high pressure and temperature [1]. It consists of a high-pressure section – the driver section, and a low-pressure section – the driven section, separated by a flange section containing a physical diaphragm. Pressure transducers are fitted along the length – two static pressure transducers in each of the sections, and two dynamic pressure transducers in known locations along the low-pressure section. An air hose connected to a high-pressure reservoir can be attached to the high-pressure end of the shock tube, increasing the pressure within to a magnitude that causes the diaphragm to burst. This results in a rapid equalization between the

shock tube sections and induces a normal shock wave that travels the length of the tube, past the dynamic PTs. Data about the internal conditions and changes in these conditions during this process is collected by the 4 PTs and recorded for later analysis.

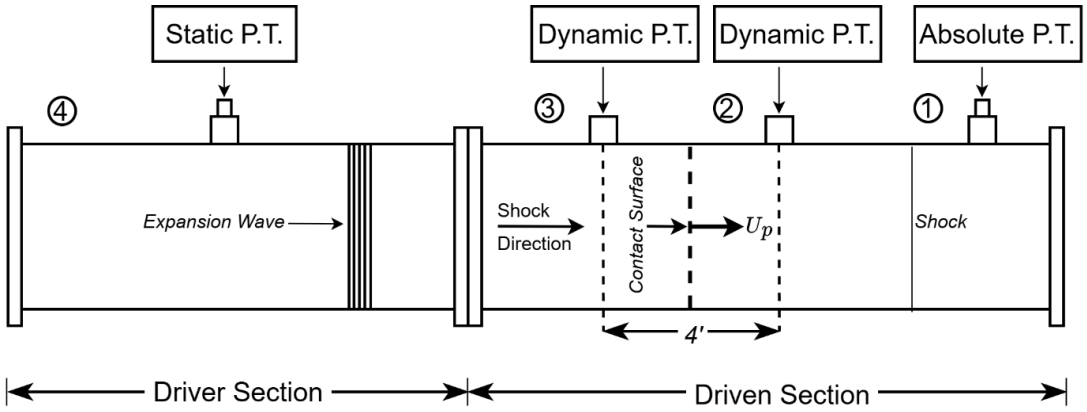

Fig. 4: Schematic of the high-speed shock tube used for experimentation. Note the two-section layout described above and the 4 pressure transducers along the length.

1. Diaphragms

The diaphragm material used to separate the shock tube sections and induce shock conditions is a key aspect of this procedure. Three different diaphragms were tested: single-ply aluminum foil, 2-mil mylar plastic, and 5-mil mylar plastic, where 'mil' refers to the thickness in millimeters of the mylar sheet used. Different materials result in different shock conditions, as a tougher diaphragm can withstand a greater pressure differential between the sections and thus will induce a stronger shock condition when it ruptures.

2. Pressure transducer

A pressure transducer (PT) measures the difference between two pressure values and writes a proportional output in volts. Two different types of pressure transducers were used, as seen in Fig. [1]: the static and absolute PTs both read differences in static pressure; the 'absolute' PT measures total pressure relative to a perfect vacuum, and the 'static' PT measures gauge pressure relative to the ambient static pressure. The dynamic PT is a variation of the static PT in that it measures a pressure difference, but it only measures pressure differences that happen because of dynamic flow conditions.

3. Digital thermocouple

A digital thermocouple is a digital measurement device that measures temperatures in degrees Celsius. The device consists of two conductors of different metals - the hot and the cold junction. When the hot junction is heated, it generates a voltage proportional to the temperature difference between the plates. This measurement is integral to determining the conditions of the atmosphere inside of the lab.

4. Data acquisition system

The data acquisition (DAQ) system functions to record instrument readings from the lab equipment. LabVIEW is the software component of the DAQ running on the lab computer and functions as the interface between the lab equipment and its operators. The purpose of LabVIEW and the DAQ is multi-faceted: it serves not only to visualize instrument readings, but also performs signal conditioning & filtering, conversions from volts to pascals, records testing time, and organizes & stores the recorded data for later analysis.

B. Data Collection

The data collection procedure involves taking measurements of the ambient conditions and equipment specifications, configuring the DAQ and LabVIEW software to record instrument readings, performing the steps to collect the data for each material, and processing the collected data for analysis and presentation. Details of this procedure can be found next:

1. Part 1: Measuring ambient conditions

For the first part of the data collection, the ambient air conditions must be determined. This is done by taking measurements of the static gauge pressure and the temperature inside the lab using the pressure transducer and digital thermocouple, respectively. These measurements are used as reference values for the internal conditions immediately after the tube is sealed, before pressurization and shock. These measurements also allow the ambient air density and local sound speed to be calculated, which will be used later for data processing. The governing equation here is the fundamental ideal gas law, which relates pressure, volume, temperature, matter, and the universal gas constant. This equation can be rearranged by expanding the term representing matter into mass over molar mass, m/M, defining the specific gas constant R as $\mathcal{R}/M$, dividing by volume, and introducing density as $m/\mathcal{V}$, seen below. This yields Eq. [1] for density:

$$\mathrm{p}\mathcal{V} = \mathrm{n}\mathcal{R}\mathrm{T} \rightarrow p = \frac{\mathrm{m}\mathcal{R}}{M\mathcal{V}} \cdot \mathrm{T} \rightarrow p = \frac{\mathrm{m}}{\mathcal{V}} \cdot \frac{\mathcal{R}}{M} \cdot \mathrm{T} \rightarrow p = \rho RT$$

$$\rho = \frac{p}{RT} \qquad [1]$$

Where the specific gas constant is known for air, $R_{air} = R = 287\,J/kg \cdot K$. The uncertainty associated with this measurement is found using the Gaussian error propagation formula, the partial derivatives of Eq. [1] w.r.t. p and T, and the known machine errors, δp and δT, yielding Eq. [2] for the density uncertainty:

$$\delta y = \sqrt{\sum_{i}^{n} \left(\frac{\partial y_i}{\partial x_i} \cdot \delta x_i\right)^2} \rightarrow \delta\rho = \sqrt{\left(\frac{\partial \rho}{\partial p} \cdot \delta \mathrm{p}\right)^2 + \left(\frac{\partial \rho}{\partial T} \cdot \delta \mathrm{T}\right)^2}$$

$$\delta\rho = \sqrt{\left(\frac{1}{RT} \cdot \delta p\right)^2 + \left(\frac{p}{RT^2} \cdot \delta T\right)^2} \qquad [2]$$

2. Part 2: Shock tube preparation & testing procedure

Next, the shock tube and DAQ are prepared to perform the tests. First, the exact location of the pressure transducers is measured and recorded and will be used later for data processing. The flange is unbolted and the diaphragm material is installed between the two sealing rubber gaskets. The diaphragm and seal are placed back in the flange section and all 4 bolts are tightened with wrenches to prevent leakage. The air hose is connected to the high-pressure section, first ensuring that both the source and section valves are closed. A fresh experiment is initiated in LabVIEW, checking that all instrumentation is functioning properly. The source valve is opened first to pressurize the line, and then the high-pressure inlet valve is opened *slowly* until the diaphragm bursts and induces the desired normal shock wave, after which the inlet valve is quickly closed again. The DAQ detects the burst, isolates the relevant data, and presents it in LabVIEW, from which it can be determined if the test was successful and if the desired results were obtained. The source valve is then shut off, the hose disconnects from the high-pressure section, and the inlet valve is opened again *slowly* to bleed the excess pressure from the tube. After the shock tube has reached pressure equilibrium, the flange is unbolted again to retrieve the remnants of the diaphragm.

This procedure is repeated for each diaphragm material tested, i.e. single-ply aluminum and the 3-mil & 5-mil mylar plastic, and the relevant data is extracted from the lab computer for processing and analysis.

C. Data Processing

The data processing procedure involves understanding the format of the DAQ output and other relevant facts about the equipment, understanding the underlying theory and key equations & derivations, and applying these theories & equations to manipulate the experimental data. Quantities at a specific location will be denoted with numerical subscripts 1-4, corresponding to stations 1-4 seen in Fig. [4]. Experimentally computed quantities will be denoted with the subscript exp. Analytically computed quantities will be denoted with the subscript ana.

1. Part 1: Important derivations

To derive the necessary relations, consider the mass continuity, momentum, and energy equations for one-dimensional flow in the shock frame:

$$\rho_1 W = \rho_2 (W - u_p) \qquad [3.1]$$

$$p_1 + \rho_1 W^2 = p_2 + \rho_2 (W - u_p)^2 \qquad [4.1]$$

$$h_1 + W^2/2 = h_2 + (W - u_p)^2/2 \qquad [5.1]$$

These equations govern normal shocks moving into stagnant gas. Eqs. [3.1-5.1] can be rearranged for shock speed, contact surface speed, and the differential speed:

$$W - u_p = W \cdot \frac{\rho_1}{\rho_2} \quad [3.2]$$

$$W = (W - u_p) \cdot \frac{\rho_2}{\rho_1} \quad [4.2]$$

$$u_p = W\left(1 - \frac{\rho_1}{\rho_2}\right) \quad [5.2]$$

Eq. [3.2] can be used in Eq. [4.1], and then rearranging for shock speed W:

$$p_1 + \rho_1 W^2 = p_2 + \rho_2 W^2 \cdot \left(\frac{\rho_1}{\rho_2}\right)^2$$

$$p_2 - p_1 = W^2\left[\rho_1 - \rho_2\left(\frac{\rho_1}{\rho_2}\right)^2\right] \cdot \frac{\rho_1}{\rho_1} = \rho_1 W^2\left[1 - \frac{\rho_1}{\rho_2}\right]$$

$$W^2 = \frac{p_2 - p_1}{\rho_1\left[1 - \frac{\rho_1}{\rho_2}\right]} = \frac{p_2 - p_1}{\rho_2 - \rho_1} \cdot \frac{\rho_2}{\rho_1} \quad [6]$$

Using Eq. [4.2] in Eq. [6]:

$$(W - u_p)^2 \cdot \left(\frac{\rho_2}{\rho_1}\right)^2 = \frac{p_2 - p_1}{\rho_2 - \rho_1} \cdot \frac{\rho_2}{\rho_1}$$

$$(W - u_p)^2 = \frac{p_2 - p_1}{\rho_2 - \rho_1} \cdot \frac{\rho_1}{\rho_2} \quad [7]$$

With Eq. [6] for shock speed and Eq. [7] for velocity differential, substitute into Eq. [5.1], replacing the enthalpy terms h with the equivalent expression $e + \frac{p}{\rho}$:

$$e_1 + \frac{p_1}{\rho_1} + \frac{W^2}{2} = e_2 + \frac{p_2}{\rho_2} + \frac{(W - u_p)^2}{2}$$

$$e_1 + \frac{p_1}{\rho_1} + \frac{\frac{p_2 - p_1}{\rho_2 - \rho_1} \cdot \frac{\rho_2}{\rho_1}}{2} = e_2 + \frac{p_2}{\rho_2} + \frac{\frac{p_2 - p_1}{\rho_2 - \rho_1} \cdot \frac{\rho_1}{\rho_2}}{2}$$

This can be simplified to obtain Eq. [1.6] for the internal energy differential $e_2 - e_1$, where specific volume v is the inverse of density:

$$e_2 - e_1 = \frac{p_1 + p_2}{2} \cdot (v_1 - v_2) \quad [8]$$

This is the Hugoniot equation derivation w.r.t. parameters associated with moving shocks. Assuming ideal gases, where $e = c_v T$ and $v = \frac{RT}{p}$, temperature and density relations can be derived in terms of the ratio of pressures $\frac{p_2}{p_1}$ rather than Mach number, and the ratio of specific heats γ:

$$c_v T_2 - c_v T_1 = \frac{p_1 + p_2}{2} \cdot \left(\frac{RT_1}{p_1} - \frac{RT_2}{p_2}\right)$$

Knowing $c_v = \frac{R}{\gamma - 1}$ and simplifying:

$$\frac{RT_2}{\gamma - 1} - \frac{RT_1}{\gamma - 1} = \frac{p_1 + p_2}{2} \cdot \left(\frac{RT_1}{p_1} - \frac{RT_2}{p_2}\right)$$

$$\frac{T_2}{T_1} = \frac{\left(\frac{p_2}{p_1} + \frac{1}{\gamma - 1} + 1\right)}{\left(\frac{p_1}{p_2} + \frac{1}{\gamma - 1} + 1\right)} = \frac{p_2}{p_1} \cdot \frac{\gamma p_1 - p_2 + \gamma p_2}{\gamma p_1 - p_1 + \gamma p_2} = \frac{p_2}{p_1} \cdot \left[\frac{\frac{\gamma + 1}{\gamma - 1} + \frac{p_2}{p_1}}{1 + \frac{\gamma + 1}{\gamma - 1} \cdot \frac{p_2}{p_1}}\right] \quad [9]$$

Using this in the equation of state for an ideal gas, $\rho = \frac{P}{RT}$:

$$\frac{\rho_2}{\rho_1} = \frac{p_2}{p_1} \cdot \frac{T_1}{T_2} = \frac{1 + \frac{\gamma + 1}{\gamma - 1} \cdot \frac{p_2}{p_1}}{\frac{\gamma + 1}{\gamma - 1} + \frac{p_2}{p_1}} \quad [10]$$

Consider this Mach number to be the shock Mach number:

$$M_s = \frac{W}{a_1} \quad [11]$$

Where flow speed u is replaced by shock speed W, and a_1 is the upstream speed of sound or the speed of sound in the stationary ahead of the shock, given by:

$$a_1 = \sqrt{\gamma_a R T_a} \quad [12]$$

The pressure ratio across the contact surface can be rearranged for shock Mach number:

$$\frac{p_2}{p_1} = 1 + \frac{2\gamma}{\gamma+1} \cdot (M_s^2 - 1)$$

$$M_s = \sqrt{\frac{\gamma+1}{2\gamma} \cdot \left(\frac{p_2}{p_1} - 1\right) + 1} \quad [13]$$

Equating Eq. [13] to Eq. [11] allows us to solve for shock speed W in terms of the specific heat of the driven section, and the pressure ratio:

$$\frac{W}{a_1} = \sqrt{\frac{\gamma+1}{2\gamma} \cdot \left(\frac{p_2}{p_1} - 1\right) + 1}$$

$$W = a_1 \cdot \sqrt{\frac{\gamma+1}{2\gamma} \cdot \left(\frac{p_2}{p_1} - 1\right) + 1} \quad [14]$$

Finally, substituting Eq. [14] and Eq. [10] into Eq. [5.2] for contact surface speed:

$$u_p = W\left(1 - \frac{\rho_1}{\rho_2}\right) \quad [5.2]$$

$$u_p = W \cdot \left(1 - \left(\frac{1 + \frac{\gamma+1}{\gamma-1} \cdot \frac{p_2}{p_1}}{\frac{\gamma+1}{\gamma-1} + \frac{p_2}{p_1}}\right)^{-1}\right)$$

$$u_p = \frac{a_1}{\gamma} \cdot \left(\frac{p_2}{p_1} - 1\right) \sqrt{\frac{\frac{2\gamma}{\gamma+1}}{\frac{p_2}{p_1} + \frac{\gamma-1}{\gamma+1}}} \quad [15]$$

2. Part 2: Theory and preparation

The DAQ presented the collected data in text files containing the following information: the sampling rate, which is set at $40\,kHz$, the driven section pressure in $psia$, the driver section pressure in $psig$, and the pressure at each of the dynamic pressure transducers in volts. Beginning with the experimental calculations: the speed at which the normal shock wave travels, W, can be computed as a function of the sampling rate f, the measured distance between the dynamic PTs Δx, and the number of data points m in the range of interest. Eq. [16] is used to determine the experimental shock speed W_{exp}:

$$W_{exp} = \frac{\Delta x}{\Delta t} \quad [16]$$

The uncertainty associated with this measurement is found using the gaussian error propagation formula, the partial derivatives of Eq. [16] w.r.t. Δx and ΔT, and the known errors, δx and δt, yielding Eq. [17] for the shock speed uncertainty:

$$\delta y = \sqrt{\sum_i^n \left(\frac{\partial y_i}{\partial x_i} \cdot \delta x_i\right)^2} \rightarrow \delta \mathrm{W_{exp}} = \sqrt{\left(\frac{\partial \mathrm{W_{exp}}}{\partial \Delta \mathrm{x}} \cdot \delta \mathrm{x}\right)^2 + \left(\frac{\partial \mathrm{W_{exp}}}{\partial \Delta \mathrm{t}} \cdot \delta \mathrm{t}\right)^2}$$

$$\delta \mathrm{W_{exp}} = \sqrt{\left(\frac{1}{\Delta t} \cdot \delta \mathrm{x}\right)^2 + \left(-\frac{\Delta x}{\Delta t^2} \cdot \delta \mathrm{t}\right)^2} \quad [17]$$

The pressure ratio across the normal shock wave can be computed analytically as a function of the pressure ratio between stations 2 and 1, $\frac{p_2}{p_1}$, the local speed of sound at station 1, a_1, and the known ratio of specific heats for air, $\gamma_{air} = \gamma = 1.4$. First, Eq. [18] is used to determine the experimental pressure ratio $\frac{p_{2,exp}}{p_1}$:

$$\frac{p_{2,exp}}{p_1} = \frac{p_1 + \Delta p}{p_1} \rightarrow p_{2,exp} = p_1 + \Delta p \quad [18]$$

Where Δp is the differential pressure between the dynamic PTs obtained from the data file. Then Eq. [19] can be used to determine the initial speed of sound in the driver section, $a_{4,exp}$:

$$a_{4,exp} = \frac{W_{exp}}{\sqrt{\frac{\gamma+1}{2\cdot\gamma}\left(\frac{p_{2,exp}}{p_1}-1\right)+1}} \quad [19]$$

Note that the speed of sound in both the driver and the driven sections is assumed to be equal, i.e. $a_1 = a_4 = a$. Next, the contact surface velocity u_p can be computed as a function of sound speed a, specific heat ratio γ, and the pressure ratio computed above, $\frac{p_2}{p_1}$. Eq. [20] is used to determine the experimental contact surface velocity:

$$u_{p,exp} = \frac{a_{exp}}{\gamma}\cdot\left[\frac{p_{2,exp}}{p_1}-1\right]\cdot\sqrt{\frac{\frac{2\gamma}{\gamma+1}}{\frac{p_{2,exp}}{p_1}+\frac{\gamma-1}{\gamma+1}}} \quad [20]$$

Next, the analytical calculations: the speed of sound a can be computed as a function of the ambient temperature T, the known specific gas constant for air R and the known ratio of specific heats for air γ. Eq. [21] is used to determine the analytical speed of sound:

$$a_{ana} = \sqrt{\gamma RT} \quad [21]$$

The assumption that the speed of sound does not change applies to the analytical calculations as well. The reference pressure ratio across the shock wave, $\frac{p_2}{p_1}$, can be computed using thermodynamic properties in the form of the known normal shock jump relations. The analytical reference pressure ratio, $\frac{p_{2,ana}}{p_1}$, across the shock is given in Eq. [22] as a function of the ratio of specific heats γ and the Mach number M_s:

$$\frac{p_{2,ana}}{p_1} = 1+\frac{2\gamma}{\gamma+1}\cdot(M_s^2-1) \quad [22]$$

Where the Mach number can be found from the experimental shock speed W_{exp} and the analytical speed of sound a_{ana}, as seen in Eq. [23]:

$$M_s = \frac{W_{exp}}{a_{ana}} \quad [23]$$

The analytical shock speed W_{ana} is then computed as a function of the quantities just calculated by using Eq. [24]:

$$W_{ana} = a_{ana}\cdot\sqrt{\frac{\gamma+1}{2\gamma}\left[\frac{p_{2,ana}}{p_1}-1\right]+1} \quad [24]$$

The pressure ratio across the shock, $\frac{p_4}{p_1}$, can then be computed as a function of the reference pressure ratio $\frac{p_2}{p_1}$, the speed of sound a, and the ratio of specific heats γ. Eq. [25] is used to compute the analytical pressure ratio across the shock:

$$\frac{p_4}{p_1} = \left(\frac{p_{2,ana}}{p_1}\right)\cdot\left[1-\frac{(\gamma-1)\cdot\left(\frac{a_{1,ana}}{a_{4,ana}}\right)\cdot\left(\frac{p_{2,ana}}{p_1}-1\right)}{\sqrt{2\gamma\cdot\left[2\gamma+(\gamma+1)\cdot\left(\frac{p_{2,ana}}{p_1}-1\right)\right]}}\right]^{-\left(\frac{2\gamma}{\gamma-1}\right)} \quad [25]$$

The contact surface velocity can be found using an equation of the same form as Eq. [20] - the equation used for the experimental contact surface velocity - by substituting the experimental values for the analytical values just computed. Eq. [26] is used to compute the analytical contact surface velocity:

$$u_{p,ana} = \frac{a_{ana}}{\gamma}\cdot\left[\frac{p_{2,ana}}{p_1}-1\right]\cdot\sqrt{\frac{\frac{2\gamma}{\gamma+1}}{\frac{p_{2,ana}}{p_1}+\frac{\gamma-1}{\gamma+1}}} \quad [26]$$

These are the fundamental equations and underlying theoretical concepts that support the procedure followed to process the experimental data, extract the desired quantities, and present the relevant findings.

3. Part 3: Processing, calculations, and presentation

Data pre-processing and calculation procedures were done using MATLAB, and the following procedure was followed for each diaphragm material data file. First, the output file is obtained from the DAQ and read to extract the four-column vectors of data, i.e. the measurements from each PT. The desired range is truncated to remove leading data points collected before the diaphragm bursts, as it contains no useful information. Variables are defined for the

measured ambient conditions, shock tube dimensions, known constants, and the known machine errors. Symbolic equations and the required symbolic variables are defined for Eqs. [16-26], ensuring to denote elementwise operations. The necessary symbolic operations are performed, e.g. the partial derivative terms for error propagation, before local function handles are created to evaluate these symbolic equations numerically. The relevant refined data vectors are passed through these functions to compute the desired quantities, which are then stored for analysis and presentation. Figures are created and populated to present the computed quantities, including static & dynamic pressure as a function of time (separately, for each material), and the pressure ratio $\frac{p_2}{p_1}$ vs. shock speed W, the contact surface velocity u_p vs. pressure ratio $\frac{p_2}{p_1}$, and the shock speed W & pressure ratio $\frac{p_2}{p_1}$ vs. the pressure ratio $\frac{p_4}{p_1}$, all of which should contain analytical and experimental points for each material, totaling 10 plots.

IV. Results

The experimental results from the lab experiment prove that static and dynamic pressure measurements show distinct trends, with rupture pressure increasing significantly for stronger diaphragm materials. Higher rupture pressures result in faster shockwave propagation, due to the increased pressure differential forcing a faster shockwave down the barrel of the test section. The generated dynamic pressure plots from the experimental data show that shockwave speed must increase with higher burst pressures, confirming the expected relationship between diaphragm material and shock strength.

The selection of proper materials for the diaphragm plays the most important part in determining rupture pressure, shockwave speed, and pressure ratios in this experiment. More rigid diaphragms like the 5mm plastic will result in significantly higher rupture pressures. The thinner aluminum diaphragm bursts at the lowest pressure and with the most uniformity.

The more rigid diaphragms did not rupture uniformly, leading to an asymmetric shockwave initiation, which is the most likely explanation for the deviations in the measured pressure ratios. Higher burst pressures also tend to create stronger and faster shockwaves, but the nonlinear rupture process can overcome this and lead to unexpected discrepancies in shock conditions or testing conditions. The ability to precisely predict the non-linear aspects is precisely why there exists a need for experimental calibration of supersonic flow devices in addition to any analytical testing that takes place.

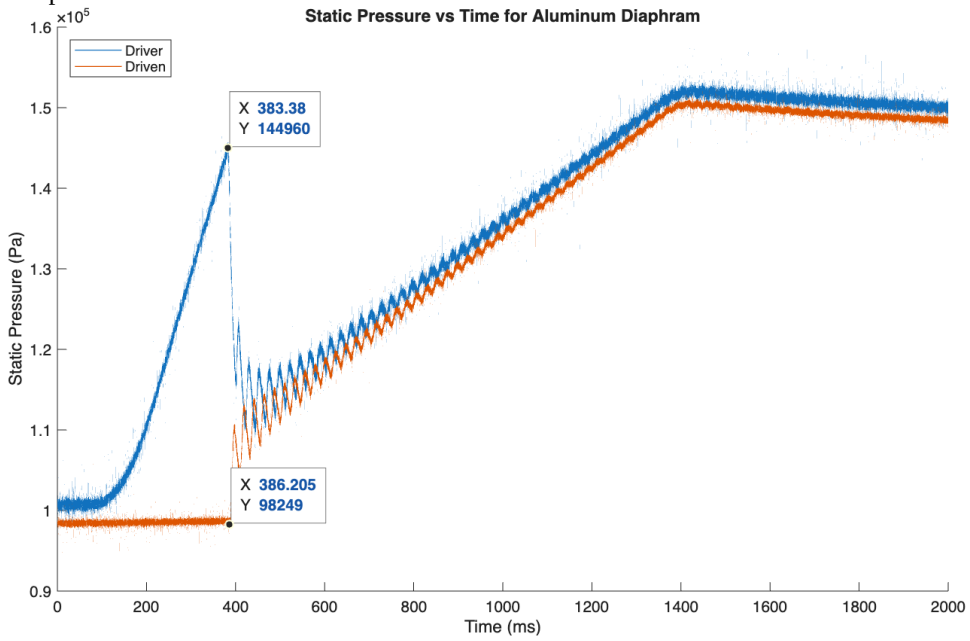

Fig. 5 Static Pressure vs. Time for Aluminum

Fig. 5 shows the static pressure at different locations in the shock tube during the aluminum burst disk experiment. The driver static pressure initially increases steeply, while the driven pressure remains constant. Once it had reached roughly 145 kPa, the diaphragm ruptured, causing a simultaneous pressure jump in both driver and driven sections

toward each other, followed by oscillations and a steady linear increase in pressure. This is precisely what can be predicted by shock propagation and pressure equalization.

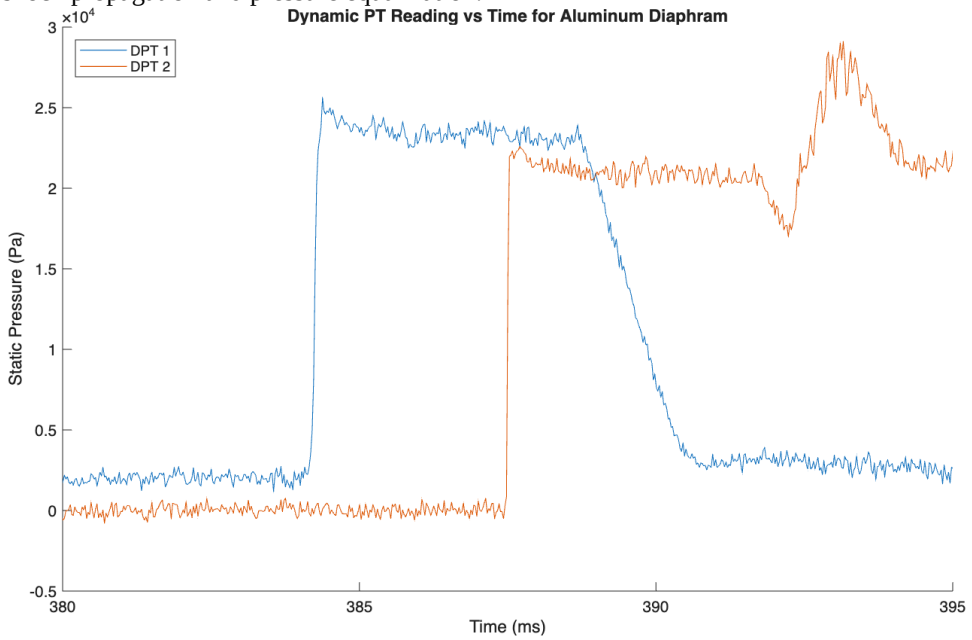

Fig. 6 Dynamic Pressure Transducer Reading vs. Time for Aluminum

Fig. 6 illustrates the dynamic pressure response at two sensor locations. DPT1 registers an initial spike from 0.25 Pa to 2.5 Pa almost instantly, while DPT2 remains unchanged for nearly 3 ms before experiencing a similar increase. This delay is caused by the physical shockwave traveling down the tube at a set speed that is determined by the pressure differential on either side of the shock and the temperature in the test section.

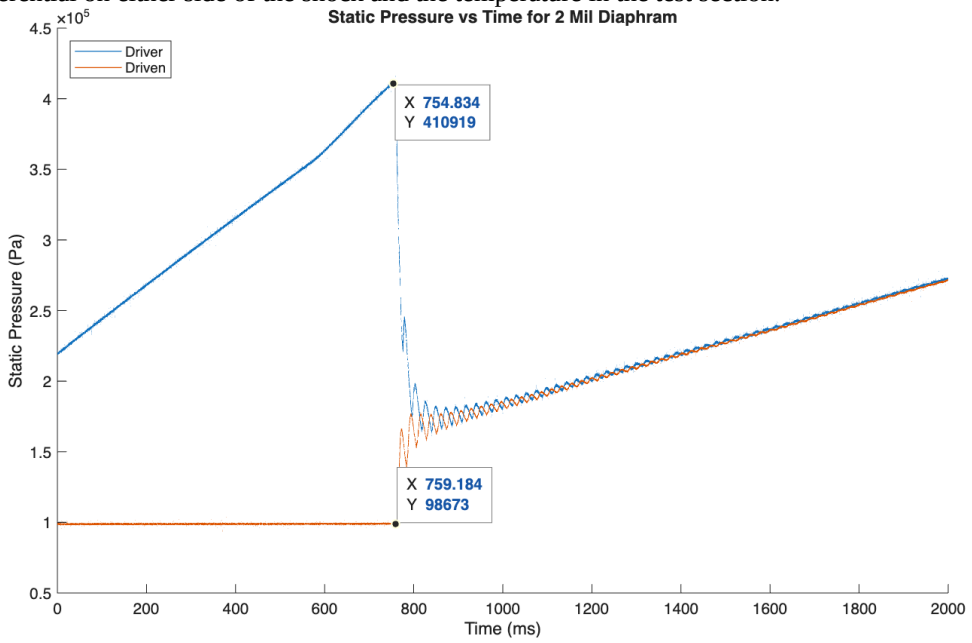

Fig. 7 Static Pressure vs. Time for 2mm Plastic

Fig. 7 ostensibly reflects the aluminum case but with the significant difference being that the rupture occurred at roughly 410 kPa instead of 145 kPa. The driver pressure increases sharply before rupture, and both pressures then experience a synchronized jump together as the bust disk pops. The oscillations post-rupture appear similar to aluminum, signifying that the pressure equalization remains relatively consistent despite material differences.

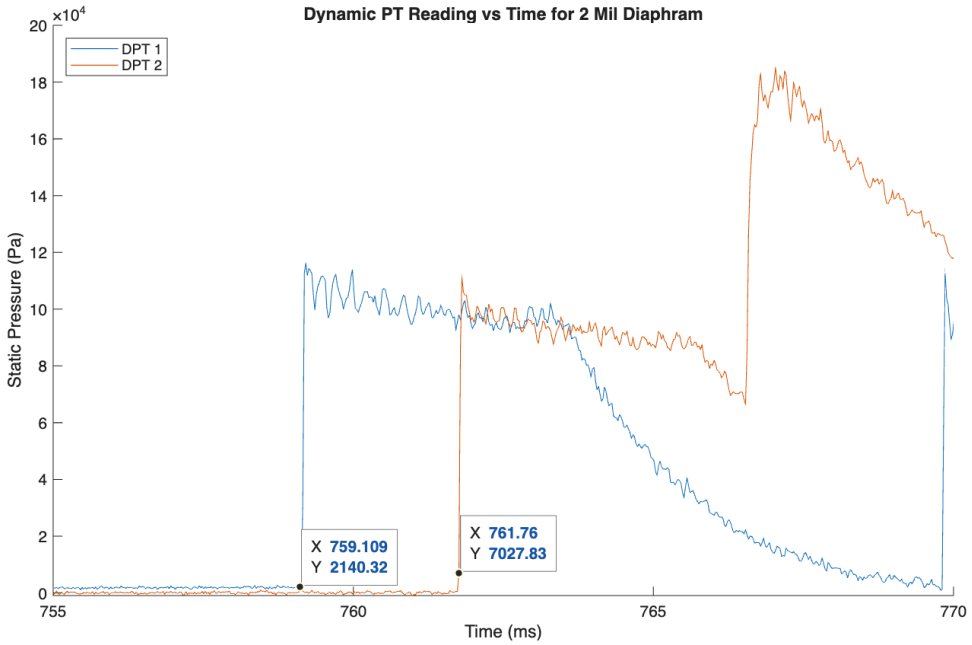

Fig. 8 Dynamic Pressure Transducer Readings vs. Time for 2mm Plastic

Similar to the aluminum case, DPT1 sees an immediate pressure jump, while DPT2 experiences a delay of roughly 2.5 ms. The shorter delay compared to aluminum suggests a faster shock propagation due to the higher burst pressure. This data aligns with the expected behavior of a shock tube.

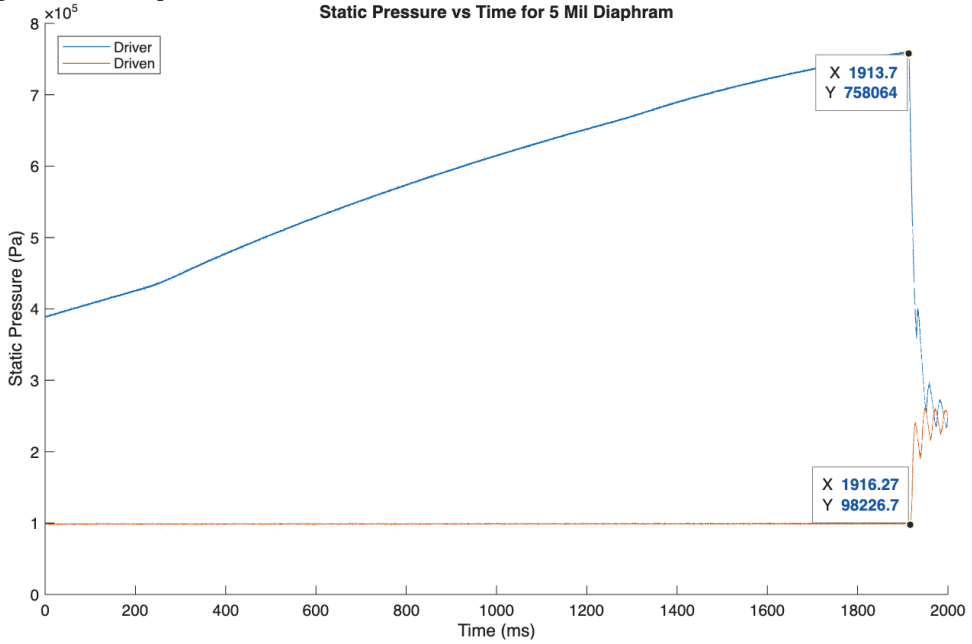

Fig. 9 Static Pressure vs. Time for 5mm Plastic

For the 5mm plastic diaphragm, the rupture occurs at 758 kPa, the highest of any of the three materials. The pressure trend remains consistent with the previous cases, with an initial steep increase, and abrupt rupture, followed by oscillations between the two as the pressure consistently rises for both driver and driven.

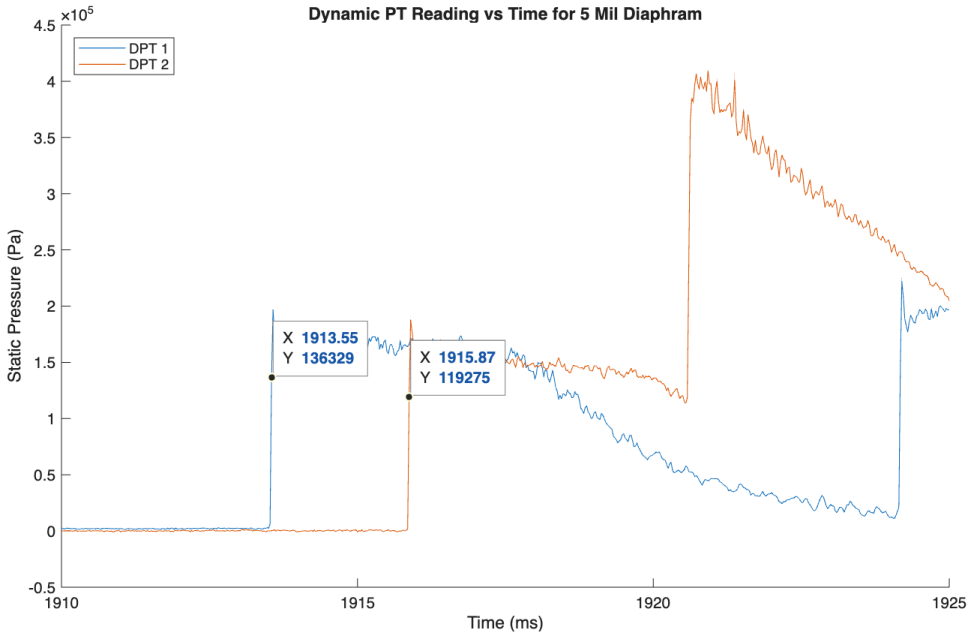

Fig 10. Dynamic Pressure Transducer Readings vs. Time for 5mm Plastic

The dynamic pressure response for 5mm plastic is similar to both the previous cases but exhibited a delay of 2.3 ms, slightly shorter even than the 2mm plastic and significantly shorter than the aluminum burst disk. This reinforces that a higher burst pressure leads to a quicker shockwave as the trend has continued across all material thicknesses.

The static pressure plots for all three materials show extremely similar trends, with a steep increase in driver static pressure until the membrane reaches the critical point and ruptures, followed by a rapid pressure equalization. The rupture pressure varies significantly between them with aluminum at 145 kPa, 2mm plastic at 410 kPa, and 5mm plastic at 758 kPa. As the diaphragm material got thicker and more rigid it was, consistently requiring higher pressures to break.

After rupture, the static pressures in the driven sections did not immediately stabilize but instead had significant oscillations between which pressure, driven or driver, was higher. These oscillations occur within the tube as the shockwave propagates and reflects off the tube edges. Additionally, the linear pressure increase following every rupture suggests that the shockwave reflection is the primary cause, compressing the gas as it ricochets inside the shock tube.

The dynamic pressure plots highlight how pressure changes over time at the different measurement locations of the experiment. DPT1, positioned closer to the diaphragm, experiences an immediate and sharp pressure jump upon rupture, indicating the arrival of the shockwave. DPT2, located farther down the tube, registered a delayed response for each initial shockwave. The delay times are measured as 3 ms for aluminum, 2.5 ms for 2mm plastic, and 2.3 ms for 5mm plastic, trending with stronger diaphragms producing faster-moving shockwaves that reduce the time lag between sensors.

This decreasing delay with increasing burst pressure experimental proves that a higher initial pressure difference across the membrane results in a faster shockwave. The magnitude of the pressure jump also varies between materials. Stronger diaphragms have more significant increases in dynamic pressure. This is completely expected based on the analytical models, as a higher-energy shockwave induces greater pressure differentials along its path. The slight inconsistencies between the materials could be attributed to differences in membrane rupture uniformity, with thicker and more flexible materials having more irregular shockwave formations.

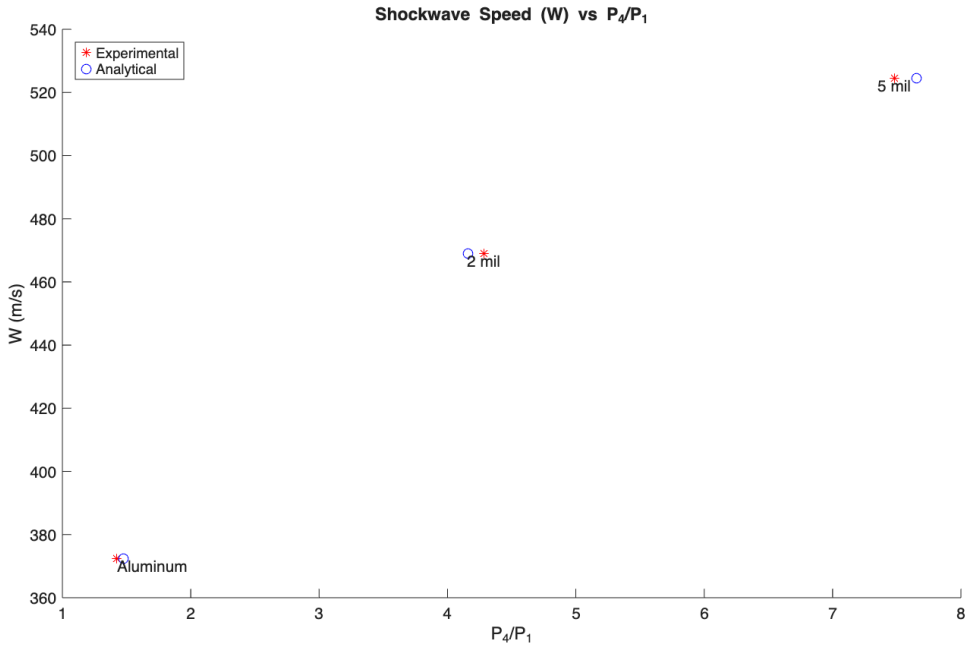

Fig. 11 Shockwave Speed vs. P4/P1 for All Materials

Fig. 11 compares experimental and analytical shockwave speeds across different materials. Aluminum shows the closest agreement with analytical predictions, while 2mm plastic has a slightly higher P4/P1 and 5mm plastic has a slightly lower P4/P1. The data signifies that the diaphragm stiffness affects shockwave propagation speed.

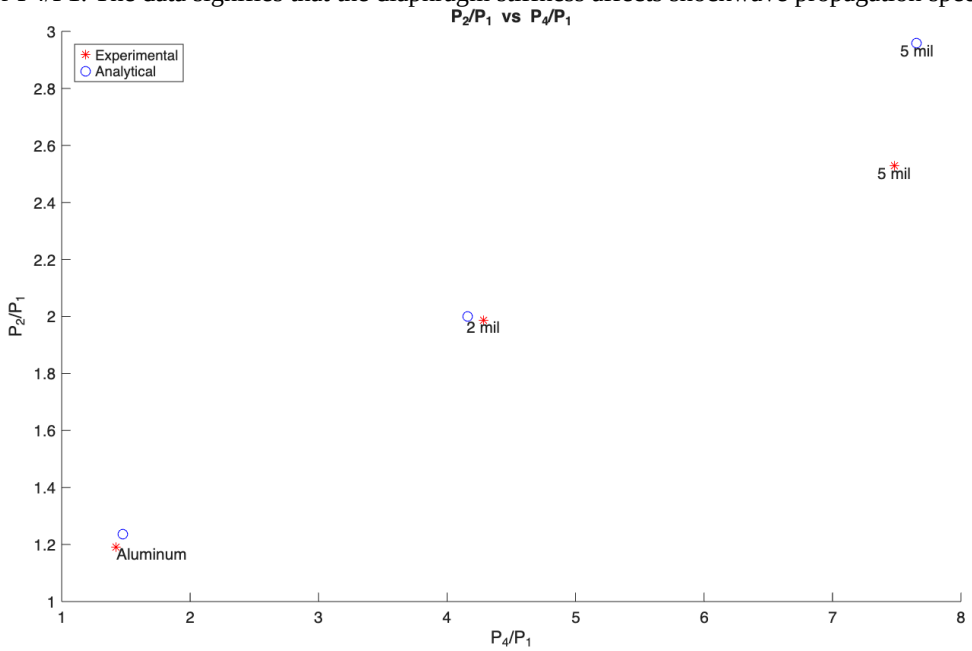

Fig. 12 P2/P1 vs. P4/P1 for All Materials

Fig. 12 shows how P2/P1 relates to P4/P1 for each material. Aluminum's experimental P2/P1 is slightly lower than analytical values, while 2mm plastic shows a slight overestimation of P4/P1. The 5mm plastic, however, significantly underpredicts P2/P1, suggesting that material stiffness affects pressure transmission across the shock front.

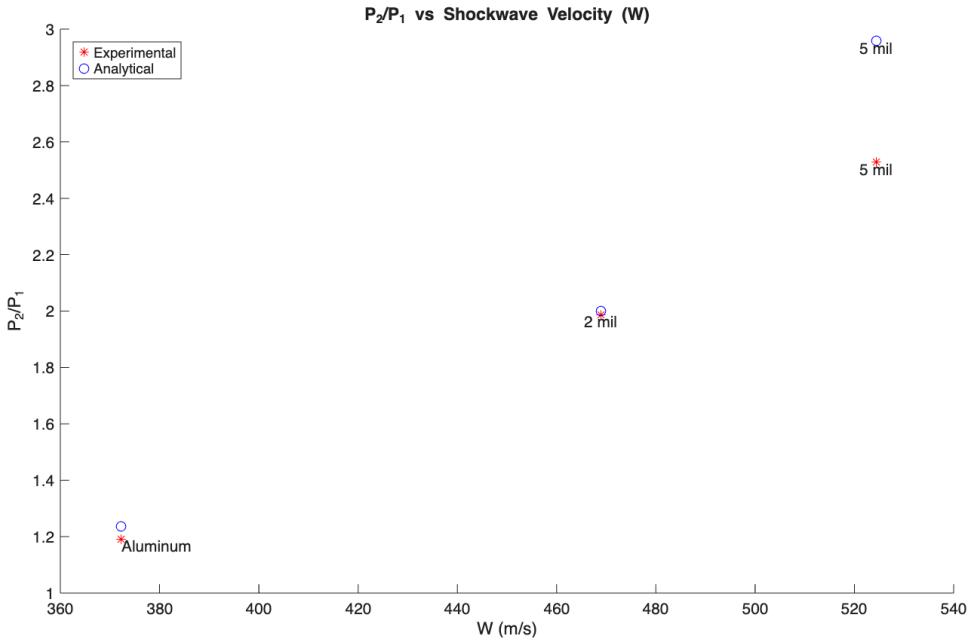

Fig. 13 P2/P1 vs. Shockwave Speed for All Materials

Fig. 13 shows the positive correlation between P2/P1 and shockwave speed. Higher pressure ratios drive stronger shockwaves. However, for 5mm plastic, the assumptions made in the analytical modeling clearly do not reflect the situational reality as they over-predict P2/P1. The results once again highlight the significance of material choice on shock propagation.

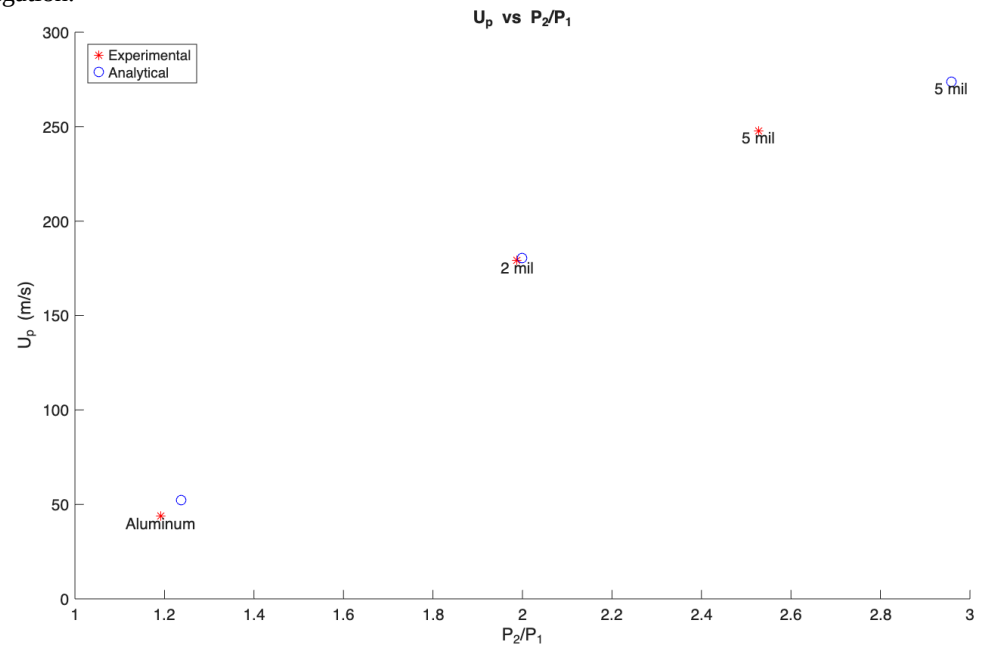

Fig. 14 Up vs. P2/P1 for All Materials

Fig. 14 demonstrates that contact surface velocity U_p is proportional to P2/P1. Aluminum's data is slightly below analytical predictions, while 5mm plastic significantly deviates in both U_p and P2/P1. The data shows that the rupture behavior of the burst disk impacts the downstream contact surface velocity and shock interactions.

Overall, the experimental results were closely aligned with the analytical predictions, though notable deviations occurred especially for the 5mm plastic diaphragm. The 2mm plastic exhibited the closest agreement, showing its rupture behavior is well-approximated by the theoretical model. 5mm plastic on the other hand shows significant deviations in both P2/P1 and U_p, which may stem from the rupture occurring over time rather than instantly,

unaccounted-for material flexing, or shockwave reflections off of the wall of the tube affecting pressure measurements.

The most significant cause of the deviations is that the analytical model assumes an idealized, instantaneous rupture. In reality, the diaphragm does not break perfectly evenly. The rupture process in stronger materials can create disturbances that affect the shock propagation, leading to cascading differences between the expected and observed results for these thicker and stronger materials. Solving these discrepancies would require reducing the number of assumptions in the model and possibly incorporating experimental correction factors, this would improve predictive accuracy for different diaphragm materials if they were adjusted accordingly.

The experimental results suggest that the initial speed of sound in the test section of the shock tube remains mostly constant, though minor deviations from analytical expectations were observed. These discrepancies could have arisen from minor temperature fluctuations inside the tube, or even minor pressure losses in the system through the valves or bolts holding the tube together. Since the speed of sound is given by Eq. 12, any changes in temperature or the ratio of specific heats will influence wave propagation speed.

While the shock tube is designed to maintain controlled conditions, even slight heating from compression effects from reflected shock waves or imperfections in diaphragm rupture can cause variations in the speed of sound.

There are two primary methods for altering the speed of sound in the shock tube. The first is to change the gas composition, as the speed of sound is highly dependent on the gas medium. Helium and hydrogen exhibit much higher speeds of sound than air or nitrogen. Using lighter gases would increase the value of a, reducing the Mach number for any given velocity. The second way would be to modify the temperature, since as can be seen in Eq. 12, increasing temperature raises the speed of sound. This can be done by preheating the gas before the experiment or by adding a heating element to the setup of the shock tube. Both methods will change shockwave formation and propagation. A higher value will result in a weaker shockwave for the same initial conditions, which would also change how well the experimental results match the theoretical predictions.

Changing the speed of sound directly impacts shockwave velocity, Mach number, and the fundamental shock tube relationships, as described by Equation 5 on the board. A higher speed of sound results in a lower Mach number for a given shockwave velocity, effectively altering the pressure and velocity profiles within the tube. Since the Mach number is defined as $M = W / a$, where W is the shockwave speed, increasing a value reduces M for the same shock velocity.

Based on the paper by Kim et al., at least two design modifications could be implemented to refine experimental results and better control shockwave behavior including gradually expanding the tube [3]. Introducing a gradual expansion in the test section could help reduce wave reflections, leading to cleaner data and fewer oscillations in pressure measurements across the length of the test section. There could also be a variable diaphragm thickness implemented into the test. Instead of a uniform-thickness diaphragm, using a pre-scored or multi-layered membrane could enable more predictable rupture behavior, improving consistency across trials. These would serve to make the rupture closer to instantaneous. These changes could mitigate pressure fluctuations and improve the similarity between experimental and analytical data. There could also be an adjustment to refining the method of diaphragm rupture such as using controlled puncturing instead of pressure burst which could reduce discrepancies in shockwave initiation, further increasing the accuracy of the experiment.

While the experimental results align closely with analytical predictions, deviations are most pronounced for 5mm plastic, likely due to the diaphragm rupture not happening uniformly across the material. The aluminum diaphragm shows the best agreement with theoretical models, suggesting it produces a more predictable and uniform shockwave. This would also line up with the idea that a material more capable of uniformly separating will produce a more uniform shock wave.

The results of the experiment prove that an analytical model will predict the broad pattern of the material reaction in a shock tube but experimental factors such as diaphragm deformation, shock reflections, and imperfect rupture conditions introduce discrepancies.

V. Conclusions

The experimental results largely confirmed our initial expectations while also revealing several small discrepancies that need some further investigation. In the static pressure plots, we observed the anticipated steep rise in driver pressure until the diaphragm ruptured, followed by a rapid oscillation of the pressure equalizing within the shock tube. This behavior aligns well with what we expected the dynamics of shock propagation to look like. In the dynamic pressure plots, the immediate, sharp pressure jump recorded by sensors closest to the diaphragm and the subsequent

delayed response from sensors further downstream illustrate the predicted relationship between burst pressure and shockwave speed. This confirms our assumption that a shockwave would be present within the shock tube. To be specific, higher burst pressures, as seen with thicker diaphragms, result in faster shockwave propagation and hence a reduced delay between sensor readings.

Our analysis revealed that the diaphragm material and thickness significantly influence the overall behavior of the shockwave. Thinner diaphragms, such as aluminum, exhibited lower rupture pressures and produced more uniform shockwaves, whereas thicker materials like 2 mm and especially 5 mm plastic required higher rupture pressures and tended to rupture non-uniformly. This non-uniform rupture not only led to asymmetrical shockwave initiation but also caused deviations in both the experimental pressure ratios (P_2/P_1) and the contact surface velocities (U_p) when compared to analytical predictions. Although the experimental and analytical results for aluminum and the 2 mm plastic diaphragm showed reasonable agreement, the discrepancies observed in the 5 mm plastic case highlight the limitations of the idealized analytical model, which assumes an instantaneous and uniform rupture.

The idea that the initial speed of sound would be constant, calculated analytically, was generally supported by the experimental data, though minor deviations suggest that small temperature fluctuations or inherent system losses may have influenced the measurements. These findings demonstrate the importance of experimental calibration, especially since the analytical model, while effective in predicting broad trends, could not fully account for the complexities of real-world rupture dynamics and shockwave reflections.

The results obtained in this experiment point to several potential improvements for future experiments. Refining the diaphragm rupture method (such as by using controlled puncturing or pre-scored membranes) and redesigning the shock tube to include features like gradual expansion or a better seal where the diaphragms where placed could help minimize shockwave reflections and non-uniform rupture effects. These modifications would likely lead to a closer alignment between experimental outcomes and analytical predictions, making the shock tube a more reliable tool for studying supersonic flow phenomena. This will lead to more reliable computations in designing planes, rockets, and other machines that operate under supersonic conditions.

Appendix A: Tabular Results

Table A1 – Density & Uncertainty

Density (Kg/m^3)	Density Uncertainty
1.1415	±0.004

Table A2 – Shockwave Speed

Material	W_{exp}	ΔW_{exp}	$W_{analytical}$ (Calculated with Avg. Burst Pressure Ratio)
Aluminum	372.2748	0.0782	372.2748
2-Mil Mylar	468.9321	0.0985	468.9321
5-Mil Mylar	524.3871	0.1101	524.3871

Table A3 – Initial Speed of Sound Driven Section

Material	$a_{1, exp}$	$a_{1, analytical}$
Aluminum	339.4265	345.0702
2-Mil Mylar	344.0955	345.0702
5-Mil Mylar	320.4283	345.0702

Table A4 – Burst Pressure Ratio

Material	$P_4/P_{1, exp}$	$P_4/P_{1, analytical}$
Aluminum	1.4736	1.4254
2-Mil Mylar	4.1608	4.2822
5-Mil Mylar	7.6551	7.4812

Table A5 – Shockwave Pressure Ratio

Material	P_2/P_1	$P_2/P_{1, analytical}$ (Calculated with Avg. Burst Pressure Ratio)
Aluminum	1.2367	1.1912
2-Mil Mylar	2	1.9878
5-Mil Mylar	2.9579	2.5276

Table A6 -Contact Surface Velocity

Material	$u_{p, exp}$	$u_{p, analytical}$
Aluminum	52.3318	43.6844
2-Mil Mylar	180.3550	179.163
5-Mil Mylar	273.8326	247.7629

Appendix B: Sample Calculations

B.1 Calculation of Density

$$\rho = \frac{p}{RT} \quad [1]$$

$$\rho = \frac{97.085}{296.35 \cdot 0.287} = 1.1415\ kg/m^3$$

B.2 Calculation of Density Uncertainty

$$\delta\rho = \sqrt{\left(\frac{0.1}{0.287 \cdot 296.35}\right)^2 + \left(\frac{96.085 \cdot 1}{0.287 \cdot 296.35^2}\right)^2} = 0.0040\ \mathrm{kg}/m^3 \quad [2]$$

B.3 Calculation of Experimental Shockwave Speed

$$W_{exp} = \frac{\Delta x}{\Delta t} = \frac{1.292}{0.0033} = 372.2748 \frac{m}{s} \quad [16]$$

B.4 Experimental Calculation of experimental Pressure Ratio P2/P1

$$\frac{p_{2,exp}}{p_1} = \frac{p_1 + \Delta p}{p_1} \rightarrow p_{2,exp} = p_1 + \Delta p = 9.876 \cdot 10^4 + 2.338 \cdot 10^4 = 1.221 \cdot 10^4 \ (unitless) \quad [18]$$

B.5 Experimental speed of sound calculation

$$a_{4,exp} = \frac{W_{exp}}{\sqrt{\frac{\gamma + 1}{2 \cdot \gamma}\left(\frac{p_{2,exp}}{p_1} - 1\right) + 1}} = \frac{372.2748}{\sqrt{\frac{1.4 + 1}{2 \cdot 1.4}\left(\frac{1.221 \cdot 10^4}{9.876 \cdot 10^4} - 1\right) + 1}} = 339.4265 \frac{m}{s} \quad [19]$$

B.6 Calculation of Contact Surface Velocity

$$u_{p,exp} = \frac{a_{exp}}{\gamma} \cdot \left[\frac{p_{2,exp}}{p_1} - 1\right] \cdot \sqrt{\frac{\frac{2\gamma}{\gamma + 1}}{\frac{p_{2,exp}}{p_1} + \frac{\gamma - 1}{\gamma + 1}}} =$$

$$\frac{339.426}{1.4} \cdot \left[\frac{1.221 \cdot 10^4}{9.876 \cdot 10^4}\right] \cdot \sqrt{\frac{\frac{2.8}{1.4 + 1}}{\frac{1.221 \cdot 10^4}{9.876 \cdot 10^4} + \frac{1.4 - 1}{1.4 + 1}}} = 52.332 \frac{m}{s} \quad [20]$$

B.7 Analytical speed of sound calculation

$$a_{ana} = \sqrt{\gamma R T} = \sqrt{1.4 \cdot 287 \cdot 296.35} = 345.0702 \frac{m}{s} \quad [21]$$

B.8 Analytical Calculation of experimental Pressure Ratio P2/P1

$$\frac{p_{2,ana}}{p_1} = 1 + \frac{2\gamma}{\gamma + 1} \cdot (M_s^2 - 1) = 1 + \frac{2 \cdot 1.4}{1.4 + 1} \cdot (1.0788^2 - 1) = 1.1912 \ (unitless) \quad [22]$$

B.9 Calculation of Mach Number

$$M_s = \frac{W_{exp}}{a_{ana}} = \frac{372.2748}{345.0702} = 1.0788 \ (unitless) \quad [23]$$

B.10 Calculation of Analytical Shockwave Speed

$$W_{ana} = a_{ana} \cdot \sqrt{\frac{\gamma + 1}{2\gamma}\left[\frac{p_{2,ana}}{p_1} - 1\right] + 1} = 345.0702 \cdot \sqrt{\frac{1.4 + 1}{2 \cdot 1.4}[1.1912 - 1] + 1} = 372.2748 \frac{m}{s} \quad [24]$$

B.11 Analytical Calculation of experimental Pressure Ratio P4/P1

$$\frac{p_4}{p_1} = \left(\frac{p_{2,ana}}{p_1}\right) \cdot \left[1 - \frac{(\gamma - 1) \cdot \left(\frac{a_{1,ana}}{a_{4,ana}}\right) \cdot \left(\frac{p_{2,ana}}{p_1} - 1\right)}{\sqrt{2\gamma \cdot \left[2\gamma + (\gamma + 1) \cdot \left(\frac{p_{2,ana}}{p_1} - 1\right)\right]}}\right]^{-\left(\frac{2\gamma}{\gamma - 1}\right)}$$

$$\frac{p_4}{p_1} = (1.1912) \cdot \left[1 - \frac{(1.4 - 1) \cdot (1) \cdot (1.1912 - 1)}{\sqrt{2 \cdot 1.4 \cdot [2 * 1.4 + (1.4 + 1) \cdot (1.1912 - 1)]}}\right]^{-\left(\frac{2*1.4}{1.4-1}\right)} = 1.4254\ (unitless) \qquad [25]$$

B.12 Calculation of Density Uncertainty

$$u_{p,ana} = \frac{a_{ana}}{\gamma} \cdot \left[\frac{p_{2,ana}}{p_1} - 1\right] \cdot \sqrt{\frac{\frac{2\gamma}{\gamma + 1}}{\frac{p_{2,ana}}{p_1} + \frac{\gamma - 1}{\gamma + 1}}} =$$

$$u_{p,ana} = \frac{345.0702}{1.4} \cdot [1.1912 - 1] \cdot \sqrt{\frac{\frac{2 * 1.4}{1.4 + 1}}{1.1912 + \frac{1.4 - 1}{1.4 + 1}}} = 43.6844 \frac{m}{s} \qquad [26]$$

Appendix C: MATLAB Code

```
%% Define constants and import data

delP = 0.1*10^3; % Taken from machine error chart (Pa)
delT = 1; % Taken from machine error chart (K)
deltime = 2.1*10^-4; % Taken from machine error chart (s)
xdpt = 1.2192; % Distance between DPT 1 and DPT 2 (m)
T = 23.2 + 273.15; % Ambient temperature (K)
gamma = 1.4;
R = 287; %J/kg*K
Patm = 97.085*10^3; % Ambient pressure (Pa)
time = linspace(0,80000,80000).*0.025; % In milliseconds
density = Patm/(R*T); % In kg/m^3
delrho = sqrt((delP/(R*T))^2 + ((Patm/(R*T^2))*delT)^2); % Density uncertainty (kg/m^3)

% Aluminum
aldata = importdata("C:\Users\traen\Downloads\Wed_1150_B1_Al.txt"); % Aluminum data
aldriven = aldata.data(:,1).*6894.76; %Absolute psi converted to Pa (aluminum)
aldriver = aldata.data(:,2).*6894.76 + Patm; %Gage psi converted to Pa (aluminum)
alpt1 = aldata.data(:,3)./0.000003378; %Converted to Pa (aluminum)
alpt2 = aldata.data(:,4)./0.000003378; %Converted to Pa (aluminum)
% 2 mil
mil2data = importdata("C:\Users\traen\Downloads\Wed_1150_B2_2-mil.txt"); % 2 mil data
mil2driven = mil2data.data(:,1).*6894.76; %Absolute psi converted to Pa (2 mil)
mil2driver = mil2data.data(:,2).*6894.76 + Patm; %Gage psi converted to Pa (2 mil)
mil2pt1 = mil2data.data(:,3)./0.000003378; %Converted to Pa (2 mil)
mil2pt2 = mil2data.data(:,4)./0.000003378; %Converted to Pa (2 mil)
% 5 mil
mil5data = importdata("C:\Users\traen\Downloads\Wed_1150_B1_5-mil.txt"); % 5 mil data
mil5driven = mil5data.data(:,1).*6894.76; %Absolute psi converted to Pa (5 mil)
mil5driver = mil5data.data(:,2).*6894.76 + Patm; %Gage psi converted to Pa (5 mil)
mil5pt1 = mil5data.data(:,3)./0.000003378; %Converted to Pa (5 mil)
```

```
mil5pt2 = mil5data.data(:,4)./0.000003378; %Converted to Pa (5 mil)

%% Create Pressure Plots

% Driven/driver plot for aluminum
figure()
hold on
plot(time, aldriver)
plot(time,aldriven)
xlabel('Time (ms)')
ylabel('Static Pressure (Pa)')
title('Static Pressure vs Time for Aluminum Diaphram')
legend('Driver','Driven', 'Location','northwest')
set(gcf,'color','white')
set(gca, 'Color', 'w')
% Pt1/Pt2 plot for aluminum
figure()
hold on
plot(time,alpt1)
plot(time,alpt2)
xlabel('Time (ms)')
ylabel('Static Pressure (Pa)')
title('Dynamic PT Reading vs Time for Aluminum Diaphram')
legend('DPT 1','DPT 2','Location','northwest')
set(gcf,'color','white')
set(gca, 'Color', 'w')
xlim([380,395]) %CREATE LIMITS FOR RIGHT BEFORE JUMP AND RIGHT AFTER JUMP

% Driven/driver plot for 2 mil
figure()
hold on
plot(time, mil2driver)
plot(time,mil2driven)
xlabel('Time (ms)')
ylabel('Static Pressure (Pa)')
title('Static Pressure vs Time for 2 Mil Diaphram')
legend('Driver','Driven', 'Location','northwest')
set(gcf,'color','white')
set(gca, 'Color', 'w')
% Pt1/Pt2 plot for 2 mil
figure()
hold on
plot(time,mil2pt1)
plot(time,mil2pt2)
xlabel('Time (ms)')
ylabel('Static Pressure (Pa)')
title('Dynamic PT Reading vs Time for 2 Mil Diaphram')
legend('DPT 1','DPT 2','Location','northwest')
set(gcf,'color','white')
set(gca, 'Color', 'w')
xlim([755,770]) %CREATE LIMITS FOR RIGHT BEFORE JUMP AND RIGHT AFTER JUMP

% Driven/driver plot for 5 mil
figure()
hold on
plot(time, mil5driver)
```

```
plot(time,mil5driven)
xlabel('Time (ms)')
ylabel('Static Pressure (Pa)')
title('Static Pressure vs Time for 5 Mil Diaphram')
legend('Driver','Driven', 'Location','northwest')
set(gcf,'color','white')
set(gca, 'Color', 'w')
% Pt1/Pt2 plot for 5 mil
figure()
hold on
plot(time,mil5pt1)
plot(time,mil5pt2)
xlabel('Time (ms)')
ylabel('Static Pressure (Pa)')
title('Dynamic PT Reading vs Time for 5 Mil Diaphram')
legend('DPT 1','DPT 2','Location','northwest')
set(gcf,'color','white')
set(gca, 'Color', 'w')
xlim([1910,1925]) %CREATE LIMITS FOR RIGHT BEFORE JUMP AND RIGHT AFTER JUMP

% p1 is driven, p4 is driver, p3 is pt1, p2 is pt2
%% Experimental Calculations

% ALUMINUM CALCULATIONS
p1al = 98762.3; % Right before diaphram burst (Pa) (Taken from min driven)
p4al = 145540; %Right before diaphram burst (Pa) (Taken from max driver)
alp4p1ratioexp = p4al/p1al; % Experimental (p4/p1)
tdptal = 0.003275; % Time taken from DPT graphs (s)
deltaPal = 23380.65; % Pressure difference taken from DPT graphs (Pa)
Walexp = xdpt/tdptal; % Wexp for aluminum (m/s)
uncertainWal = sqrt(((xdpt/tdptal)*deltime)^2); % Uncertainty in W (m/s) *This is the same for both experimental and analytical*
P2expal = p1al + deltaPal; % Experimental P2 (Pa)
a1alexp = Walexp/(sqrt(((gamma + 1)/(2*gamma))*((P2expal/p1al)-1) + 1)); % Experimental speed of sound (a1) (m/s)
Upexpal = (a1alexp./gamma).*((P2expal./p1al) - 1).*sqrt((2*gamma./(gamma + 1))./((P2expal./p1al) + ((gamma - 1)/(gamma + 1)))); % Experimental Up (m/s)
p2p1alexp = (P2expal./p1al);

% 2 MIL CALCULATIONS
p12mil = 99253.2; % Right before diaphram burst (Pa) (Taken from min driven)
p42mil = 412972; %Right before diaphram burst (Pa) (Taken from max driver)
tdpt2mil = 0.0026; % Time taken from DPT graphs (s)
deltaP2mil = 99253.2; % Pressure difference taken from DPT graphs (Pa)
W2milexp = xdpt/tdpt2mil; % Wexp for aluminum (m/s)
uncertainW2mil = sqrt(((xdpt/tdpt2mil)*deltime)^2); % Uncertainty in W (m/s) *This is the same for both experimental and analytical*
P2exp2mil = p12mil + deltaP2mil; % Experimental P2 (Pa)
a12milexp = W2milexp/(sqrt(((gamma + 1)/(2*gamma))*((P2exp2mil/p12mil)-1) + 1)); % Experimental speed of sound (a1) (m/s)
Upexp2mil = (a12milexp./gamma).*((P2exp2mil./p12mil) - 1).*sqrt((2*gamma./(gamma + 1))./((P2exp2mil./p12mil) + ((gamma - 1)/(gamma + 1)))); % Experimental Up (m/s)
p4p1ratio2milexp = p42mil/p12mil; %Analytical (p4/p1)
p2p12milexp = (P2exp2mil./p12mil);

% 5 MIL CALCULATIONS
```

```
p15mil = 99342.6; % Right before diaphram burst (Pa)
p45mil = 760474; % Right before diaphram burst (Pa) (Taken from max driver)
tdpt5mil = 0.002325; % Time taken from DPT graphs (s)
deltaP5mil = 194502.26; % Pressure difference taken from DPT graphs (Pa)182910.31
W5milexp = xdpt/tdpt5mil; % Wexp for aluminum (m/s)
uncertainW5mil = sqrt(((xdpt/tdpt5mil)*deltime)^2); % Uncertainty in W (m/s) *This is the same for both experimental and analytical*
P2exp5mil = p15mil + deltaP5mil; % Experimental P2 (Pa)
a15milexp = W5milexp/(sqrt(((gamma + 1)/(2*gamma))*((P2exp5mil/p15mil)-1) + 1)); % Experimental speed of sound (a1) (m/s)
Upexp5mil = (a15milexp./gamma).*((P2exp5mil./p15mil) - 1).*sqrt((2*gamma./(gamma + 1))./((P2exp5mil./p15mil) + ((gamma - 1)/(gamma + 1)))); % Experimental Up (m/s)
p4p1ratio5milexp = p45mil/p15mil; %Analytical (p4/p1)
p2p15milexp = (P2exp5mil./p15mil);
%% Analytical Calculations

% ALUMINUM CALCULATIONS
a1analyticalal = sqrt(gamma*R*T); % Analytical speed of sound (a1) (m/s)
M1al = Walexp/a1analyticalal; % Analytical mach number using experimental W and analytical a1
alp2p1ratio = 1 + (2*gamma/(gamma + 1))*(M1al^2 - 1); % Analytical (p2/p1)
Walana = a1analyticalal*sqrt((((gamma + 1)/(2*gamma)).*((alp2p1ratio) - 1) + 1)); % Analytical speed of shockwave W (m/s)
alp4p1ratioana = alp2p1ratio*(1-(((gamma-1)*(alp2p1ratio-1))/sqrt(2*gamma*(2*gamma + (gamma+1)*(alp2p1ratio-1))))^(-2*gamma/(gamma-1)); %Analytical (p4/p1)
Upanalyticalal = (a1analyticalal./gamma)*((alp2p1ratio) - 1)*sqrt((2*gamma/(gamma + 1))/((alp2p1ratio) + ((gamma - 1)/(gamma + 1)))); % Analytical Up (m/s)

% 2 MIL CALCULATIONS
a1analytical2mil = sqrt(gamma*R*T); % Analytical speed of sound (a1) (m/s)
M12mil = W2milexp/a1analytical2mil; % Analytical mach number using experimental W and analytical a1
p2p1ratio2mil = 1 + (2*gamma/(gamma + 1))*(M12mil^2 - 1); % Analytical (p2/p1)
W2milana = a1analytical2mil*sqrt((((gamma + 1)/(2*gamma)).*((p2p1ratio2mil) - 1) + 1)); % Analytical speed of shockwave W (m/s)
p4p1ratio2milana = p2p1ratio2mil*(1-(((gamma-1)*(p2p1ratio2mil-1))/sqrt(2*gamma*(2*gamma + (gamma+1)*(p2p1ratio2mil-1))))^(-2*gamma/(gamma-1)); %Analytical (p4/p1)
Upanalytical2mil = (a1analytical2mil./gamma)*((p2p1ratio2mil) - 1)*sqrt((2*gamma/(gamma + 1))/((p2p1ratio2mil) + ((gamma - 1)/(gamma + 1)))); % Analytical Up (m/s)

% 5 MIL CALCULATIONS
a1analytical5mil = sqrt(gamma*R*T); % Analytical speed of sound (a1) (m/s)
M15mil = W5milexp/a1analytical5mil; % Analytical mach number using experimental W and analytical a1
p2p1ratio5mil = 1 + (2*gamma/(gamma + 1))*(M15mil^2 - 1); % Analytical (p2/p1)
W5milana = a1analytical5mil*sqrt((((gamma + 1)/(2*gamma)).*((p2p1ratio5mil) - 1) + 1)); % Analytical speed of shockwave W (m/s)
p4p1ratio5milana = p2p1ratio5mil*(1-(((gamma-1)*(p2p1ratio5mil-1))/sqrt(2*gamma*(2*gamma + (gamma+1)*(p2p1ratio5mil-1))))^(-2*gamma/(gamma-1)); %Analytical (p4/p1)
Upanalytical5mil = (a1analytical5mil./gamma)*((p2p1ratio5mil) - 1)*sqrt((2*gamma/(gamma + 1))/((p2p1ratio5mil) + ((gamma - 1)/(gamma + 1)))); % Analytical Up (m/s)

%% Data Plots

% W vs p4/p1
figure()
hold on
plot(alp4p1ratioana,Walana,'r*')
plot(alp4p1ratioexp, Walexp, 'bo')
```

```
plot(p4p1ratio2milana,W2milana,'r*')
plot(p4p1ratio2milexp, W2milexp, 'bo')
plot(p4p1ratio5milana,W5milana,'r*')
plot(p4p1ratio5milexp, W5milexp, 'bo')
text(alp4p1ratioana, Walana, 'Aluminum', 'VerticalAlignment', 'cap', 'HorizontalAlignment', 'left');
text(p4p1ratio2milana, W2milana, '2 mil', 'VerticalAlignment', 'cap', 'HorizontalAlignment', 'center');
text(p4p1ratio5milana, W5milana, '5 mil', 'VerticalAlignment', 'cap', 'HorizontalAlignment', 'center');
xlabel('P_4/P_1')
ylabel('W (m/s)')
title('Shockwave Speed (W) vs P_4/P_1')
set(gcf,'color','white')
set(gca, 'Color', 'w')
legend('Experimental','Analytical','Location','northwest')

% p2/p1 vs p4/p1
figure()
hold on
plot(alp4p1ratioana,alp2p1ratio,'r*')
plot(alp4p1ratioexp, (P2expal/p1al), 'bo')
plot(p4p1ratio2milana,p2p1ratio2mil,'r*')
plot(p4p1ratio2milexp, (P2exp2mil/p12mil), 'bo')
plot(p4p1ratio5milana,p2p1ratio5mil,'r*')
plot(p4p1ratio5milexp, (P2exp5mil/p15mil), 'bo')
text(alp4p1ratioana, alp2p1ratio, 'Aluminum', 'VerticalAlignment', 'cap', 'HorizontalAlignment', 'left');
text(p4p1ratio2milana, p2p1ratio2mil, '2 mil', 'VerticalAlignment', 'cap', 'HorizontalAlignment', 'center');
text(p4p1ratio5milana, p2p1ratio5mil, '5 mil', 'VerticalAlignment', 'cap', 'HorizontalAlignment', 'center');
text(p4p1ratio5milexp, (P2exp5mil/p15mil), '5 mil', 'VerticalAlignment', 'cap', 'HorizontalAlignment', 'center');
xlabel('P_4/P_1')
ylabel('P_2/P_1')
title('P_2/P_1 vs P_4/P_1')
set(gcf,'color','white')
set(gca, 'Color', 'w')
legend('Experimental','Analytical','Location','northwest')

% p2/p1 vs W
figure()
hold on
plot(Walana,alp2p1ratio,'r*')
plot(Walexp,(P2expal/p1al), 'bo')
plot(W2milana,p2p1ratio2mil,'r*')
plot(W2milexp,(P2exp2mil/p12mil), 'bo')
plot(W5milana,p2p1ratio5mil,'r*')
plot(W5milexp,(P2exp5mil/p15mil), 'bo')
text(Walana,alp2p1ratio,'Aluminum', 'VerticalAlignment', 'cap', 'HorizontalAlignment', 'left');
text(W2milana,p2p1ratio2mil, '2 mil', 'VerticalAlignment', 'cap', 'HorizontalAlignment', 'center');
text(W5milana, p2p1ratio5mil, '5 mil', 'VerticalAlignment', 'cap', 'HorizontalAlignment', 'center');
text(W5milexp,(P2exp5mil/p15mil), '5 mil', 'VerticalAlignment', 'cap', 'HorizontalAlignment', 'center');
xlabel('W (m/s)')
ylabel('P_2/P_1')
title('P_2/P_1 vs Shockwave Velocity (W)')
set(gcf,'color','white')
set(gca, 'Color', 'w')
legend('Experimental','Analytical','Location','northwest')

% Up vs P2/P1
figure()
```

```
hold on
plot(alp2p1ratio,Upanalyticalal,'r*')
plot((P2expal/p1al), Upexpal, 'bo')
plot(p2p1ratio2mil,Upanalytical2mil,'r*')
plot((P2exp2mil/p12mil), Upexp2mil, 'bo')
plot(p2p1ratio5mil, Upanalytical5mil,'r*')
plot((P2exp5mil/p15mil), Upexp5mil,'bo')
text(alp2p1ratio,Upanalyticalal,'Aluminum', 'VerticalAlignment', 'cap', 'HorizontalAlignment', 'center');
text(p2p1ratio2mil, Upanalytical2mil,'2 mil', 'VerticalAlignment', 'cap', 'HorizontalAlignment', 'center');
text(p2p1ratio5mil, Upanalytical5mil, '5 mil', 'VerticalAlignment', 'cap', 'HorizontalAlignment', 'center');
text((P2exp5mil/p15mil), Upexp5mil, '5 mil', 'VerticalAlignment', 'cap', 'HorizontalAlignment', 'center');
xlabel('P_2/P_1')
ylabel('U_p (m/s)')
title('U_p vs P_2/P_1')
set(gcf,'color','white')
set(gca, 'Color', 'w')
legend('Experimental','Analytical','Location','northwest')
```

Appendix D: Member Contributions

Name	Contribution
Colin McArthur	Abstract, Introduction, Editor
Nicholas Nelson	Results, Editor
Trae Nelson	Code, Nomenclature, References, Editor
Justin Ritzenthaler	Conclusion, Appendix/sample calculation, Editor
Zakary Steenhoek	Procedure, Editor

Acknowledgments

We would like to thank the AEE 362 TA's for providing us with the tools and information necessary to complete this experiment and report. We would also like to acknowledge the help that came from wonderful tools such as MATLAB and Google in providing us with resources to understand and visualize the information gathered. We also would like to thank our group members for pulling together and getting it all done on time.

References

[1] Anderson, John D. Modern Compressible Flow: With Historical Perspective. https://platform.virdocs.com/read/1542835/282/#/4/4.

[2] ScienceDirect. "Shock Tubes." *ScienceDirect Topics*, Elsevier. Available at: https://www.sciencedirect.com/topics/physics-and-astronomy/shock-tubes. Accessed: February 17, 2025.

[3] Kim, J., You, H., and Kim, C. "Shock-Capturing PID Controller for High-Order Methods with Data-Driven Gain Optimization." Journal of Computational Physics, Vol. 508, Elsevier, July 1, 2024, Article 113015. Available at: https://www.sciencedirect.com/science/article/pii/S002199912400264X. Accessed: February 17, 2025.

[4] Arizona State University. "Machine Error Chart." ASU Canvas. Available at: https://canvas.asu.edu/courses/200674/files/90846148?module_item_id=14599033. Accessed January 29, 2025.

[5] MathWorks. *MATLAB 2024a*. MathWorks, 2024.

[6] Arizona State University. "Lab 1: Experimental Investigation of the Speed of a Shock Wave" ASU Canvas. Available at: https://canvas.asu.edu/courses/200674/files/92667506?module_item_id=14753585. Accessed January 29, 2025.

[7] Arizona State University. "Wed_1150_A1_Al." Unpublished data. Available on ASU Canvas. Accessed January 29, 2024.

[8] Arizona State University. "Wed_1150_A1_2-mil." Unpublished data. Available on ASU Canvas. Accessed January 29, 2025.

[9] Arizona State University. "Wed_1150_B1_5-mil." Unpublished data. Available on ASU Canvas. Accessed January 29, 2025.